Hindawi
Mathematical Problems in Engineering
Volume 2022, Article ID 9083307, 13 pages
https://doi.org/10.1155/2022/9083307

Research Article

An Efficient Energy Management Scheme for an Islanded DC Microgrid with Hybrid VRFB System

S. Hameed[1], **I. Prabhakar Reddy**[2], **V Ganesh**[1] and **Aruna rai Vadde**[3]

[1]*Department of Electrical and Electronics Engineering, Jawaharlal Nehru Technological University, Anantapur, India*
[2]*Department of Electrical and Electronics Engineering, NBKR Institute of Science and Technology, Andhra Pradesh, India*
[3]*Department of Electrical and Computer Engineering, Debre Tabor University, Debre Tabor, Ethiopia*

Correspondence should be addressed to Aruna rai Vadde; dr.rai@dtu.edu.et

Received 22 February 2022; Revised 11 March 2022; Accepted 21 March 2022; Published 14 April 2022

Academic Editor: Albert Alexander Stonier

This paper presents an efficient energy management scheme for an islanded DC microgrid included with vanadium redox flow battery (VRFB) with supercapacitor based hybrid energy storage system for a 3-phase variable load profile. The analysed islanded DC microgrid system is composed with sources such as lithium-ion batteries, fuel cell, supercapacitors, and vanadium redox flow battery (VRFB), along with involved DC/DC (buck, boost, and bidirectional) and DC/DC converters. In this paper, an adaptive proportional plus integral (PI) control based energy management scheme is implemented. The main theme on which the performance of this system is analysed is the state of charge of energy storage devices (VRFB, supercapacitor, and Li-ion battery) and the overall efficiency of system. The voltage spikes due to sudden change in load have been regulated by using supercapacitor and Li-ion battery with VRFB. To minimize the fuel consumption, an adaptive proportional plus integral control strategy is being used. In this paper the modelling and simulations are carried out by using MATLAB/SIMULINK software to demonstrate minimizing the effect of load fluctuations with the help of supercapacitor and batteries by synchronizing it to the DC microgrid.

1. Introduction

In the modern world, when the conventional sources of energy are on the verge of their extinction and the pollution levels associated with their extensive use, it has become a serious issue. It is time we switch to the nonconventional ways at a much faster rate. In present scenario, power plants are used to generate electricity and some renewable energy sources such as wind energy and solar energy at their initial stages. The main problem associated with solar energy sources is less efficient power generation, and with wind energy, the rapid fluctuation in power generation becomes the main issue. To reduce the stress on power plants for energy requirements, microgrids have become an important alternative. They are capable of extracting power from the grids and also deliver power to the grid, if and when needed. A type of microgrid which can be used as an affordable source for isolated places is an islanded DC microgrid. They are able to extract and deliver power as per the load requirements on their own, without the aid of external grid. In this paper, an energy management scheme has been proposed for the islanded DC microgrid with VRFB as the main source for the hybrid system.

In a previous paper [1], an energy management scheme with fuel cell as the main scheme has been proposed. Fuel cells though being a very useful energy source have a significant disadvantage regarding their input. The inputs of the fuel cell are hydrogen and oxygen. Although they are easily available, their pumping into the fuel cell can become an issue. To overcome this problem, we have come up with a solution to use vanadium redox flow battery as the main supply source. Another disadvantage with fuel cells is that it cannot be recharged from the DC bus unlike Li-ion and VRFBs.

In this article, VRFBs are being used as the main source to supply power to the load, with supercapacitors (which smoothens the voltage spikes at transience) and Li-ion batteries. The vanadium redox flow battery is a type of

rechargeable battery which uses vanadium ions at different oxidation states and stores chemical potential energy by the help of oxidation-reduction process. It makes use of ability of vanadium to exist in solution in four different oxidation states. The advantages associated with vanadium redox flow battery are its durability to handle more than 15,000 cycles with a charge/discharge efficiency of 75–80 per cent and energy density of 25 Wh/Kg. In addition to this, an important advantage is its cheap capital cost. It can be inferred from previous researches that for grid application it has a cost range from 745 to 825 dollars KW/h which is half of the Li-ion battery cost. VRFBs can be used to withstand a Depth of Discharge (DOD) of around 90 percent and more. In this article, Li-ion battery stores extra energy of DC grid by the help of DC/DC buck converters.

Vanadium redox flow battery has poor response in transient conditions. To overcome this issue, its synchronization with various energy storing elements like Li-ion batteries, supercapacitors, and fuel cell is required.

Different energy management schemes (EMS) have been reported in previous papers. Some of them are as follows:

(i) State control scheme

(ii) Indistinct (fuzzy) logic strategy

(iii) Adaptive P and I control strategy

(iv) Decoupling of frequency and indistinct (fuzzy) logic

(v) Minimization of consumption strategy

The details regarding these strategies are explained in [1]. It is to be understood that the capability of the designer regarding the knowledge of various components determines the performance of the applied scheme. In this paper, adaptive proportional and integral (PI) control strategy has been discussed [1]. This strategy is mainly based on the parameter controls like SOCs of batteries, supercapacitor, and DC bus voltage. This paper deals with the adaptive P and I control strategy using VRFB as the main source along with fuel cell, supercapacitors, and Li-ion battery and is connected and synchronized with the DC microgrid. VRFB is arising as another option in contrast to ESS batteries applied to inexhaustible power age frameworks to take care of ecological and asset exhaustion issues. Right now, lithium batteries are predominantly utilized in ESS; however there is an issue that a fire mishap might happen and the life expectancy is restricted. VRFB enjoys the benefit of being reasonable for enormous limit frameworks since it has a more extended life expectancy than lithium batteries and has a limit relative to amount of electrolyte. Nonetheless, there is an impediment in that it is hard to appraise the limit because of the working qualities. Vanadium redox stream battery (VRFB) has attracted a lot of thoughts since it can truly handle the unpredictable issue of supportable power age. Regardless, the low energy thickness of VRFBs prompts massive cost, which will genuinely restrict the improvement in the field of energy storing. VRFB stream field plan and stream rate upgrade is a suitable strategy for additional creating battery execution without enormous improvement costs. This overview summarizes the basic issues of VRFB improvement, depicting the working guideline, electrochemical reaction connection, and system model of VRFB. The course of stream field plan and stream rate improvement is inspected, and the battery credits and estimations for evaluating VRFB execution are summarized. The point of convergence of the assessment is the systems for stream field plan and stream rate smoothing out and the expansive relationship of battery execution between different stream field plans. Composing assessment shows that reasonable stream field arrangement can deal with the consistency of electrolyte, further foster battery credits and estimations, and in this way work on the overall execution of VRFB and reduce the cost. In this paper, Section 2 deals with the architecture of hybrid power module, Section 3 describes component modelling, Section 4 explains the EM scheme used, and Section 5 provides simulation and experimental results.

2. Architecture of Hybrid Power Module

The architecture of hybrid power is modelled based on the requirements of energy and power for fluctuating load conditions, when the system is connected to an islanded DC microgrid. The VRFB system is used to meet the average load demand of the system, whereas the batteries (Li-ion, fuel cell) and supercapacitor are designed to help the VRFB during peak demands of continuous and transient nature, respectively. The analysis in detail regarding the selection of design and its features are not covered in this paper but can be referred from [2]. As shown in Figure 1, the VRFB of 52.6 KW (46.2 Vdc) along with a battery system which contain four battery packs (12.8 V, 40 Ah) is combined with 6-NESSCAP supercapacitor module (48.6 V, 88 F). The FC (fuel cell) power module of 12.45 KW having PEM assists VRFB. The energy of VRFB, fuel cell, and batteries are controlled through their associated DC/DC converters with the help of National Instrument Embedded Controller (NI PXI-8108). In PI controller strategy DC/DC converter uses output voltage and maximum input/output current as a reference, the battery operating system (BOS) is then used to prevent battery from overcharging, overtemperature, and overdischarge. Batteries are attached with DC bus through DC/DC converter, and in case of VRFB, a bidirectional converter is used, which helps in charging and discharging of VRFB. A resistor is also used which protects supercapacitor from overvoltage and is termed as protecting resistor.

The main elements of the hybrid power module are as follows.

(i) The vanadium redox flow battery system: It is a 52.6 KW, 46.2 Vdc with built-in two separate columns separated by a Proton Exchange Membrane (PEM). The VRFB has an in-built controller which assists the main controller.

(ii) The FC power module: A 12.45 KW 60–30 Vdc PEM system provided with liquid cooling, built-in auxiliary components which include air blower, filter, hydrogen recirculation pumps, pressure regulator, fans, and pumps for cooling is used. The

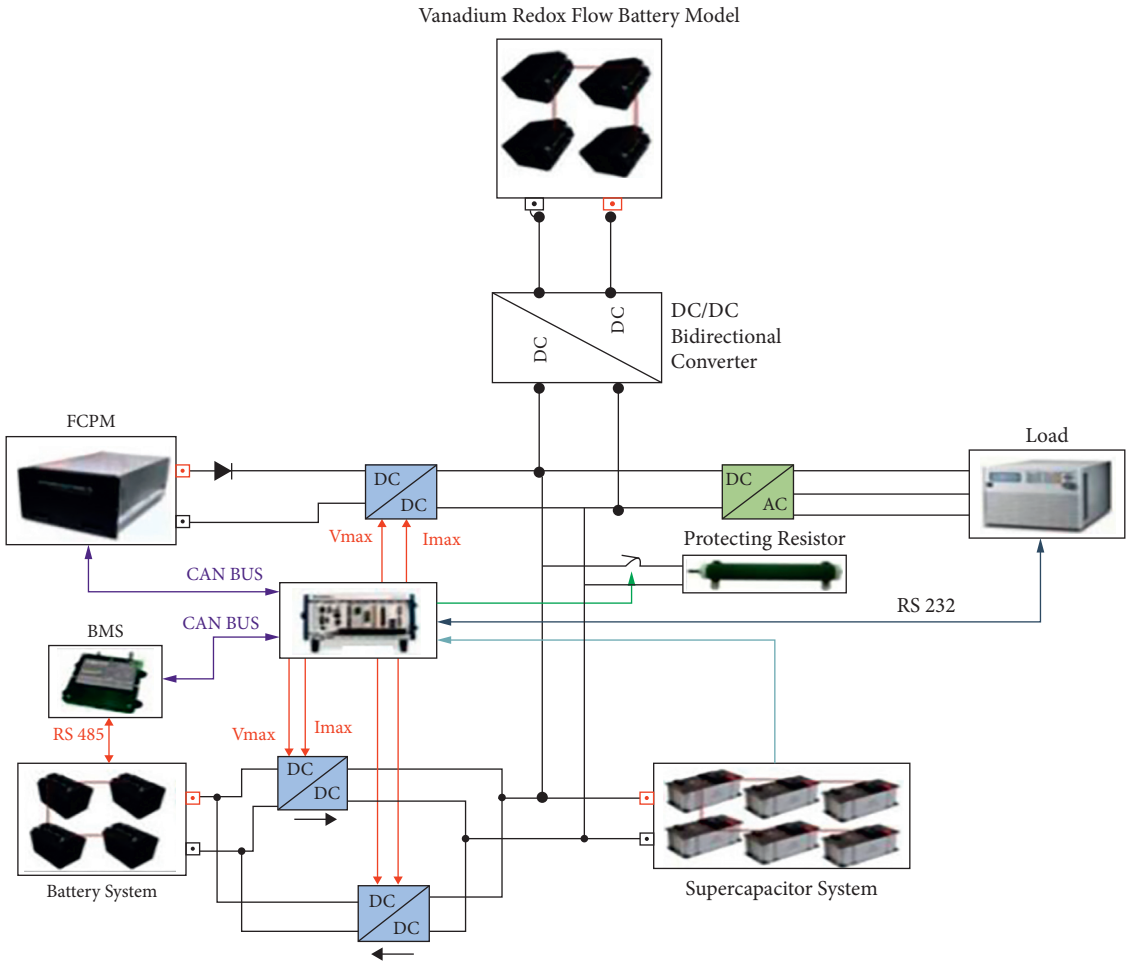

Figure 1: EM scheme for a VRFB hybrid power module.

fuel cell is equipped with its own controller for connecting to the main one.

(iii) The battery system: 4 Li-ion batteries are connected in series (12.5 KW 60–30 Vdc). Cell-to-cell balancing is provided through controllers (connected internally) to eliminate stress on individual battery and divide it uniformly to the whole battery system. This controller is then connected to the overall BMS.

(iv) The supercapacitor system: 6 supercapacitors are connected in series (48.2 V, 88 Farads) and then connections are made to a controller internally to eliminate stress on individual supercapacitor.

(v) The FC converter system: It has five DC/DC boost converters connected in parallel with 40–64 V DC input and 270 V (adjustable 243–297 V), 9.2 A DC output. Here the balancing is made possible through active current sharing.

(vi) The Li-ion converter system: Two converters, one DC/DC boost [with 40–58.2 V as DC input and 270 V, 7 A DC output] converter (for discharging of batteries) is connected in parallel with another DC/DC buck [with (243–297 V) as DC input and 48 V, 20 A DC output] converter (for charging).

(vii) The VRFB bidirectional converter system: It is used for both charging and discharging of VRFB, it acts like buck converter when charging and boost at the time of discharging (with 46.2 V as DC input and 270 V, 19 A DC output).

(viii) The inverter system: 3 DC/AC isolated converters are connected here in parallel (configuration: DC in of 160–320 V and AC output of 200 V, 400 Hz, and 5 KVA). Protection for overvoltage, short circuit, and overload is made. The output voltage of converter is then regulated to keep total harmonic distortion within three percent.

(ix) The programmable DC/AC load: Six 4.5 KW, 45 A, 350 V loads are used which can be programmed electronically.

(x) Sensor and signals conditioning: Voltage and current sensors are used at input and output of all the converters. Individual device temperature can be controlled through their controllers or thermistors.

3. Component Modelling

The study of the energy management system for an islanded DC microgrid requires that each subsystem is properly modelled with accuracy. This leads to a better understanding of the system, which allows for an effective design of the EMS. This section now describes the modelling approach of each individual component.

3.1. Vanadium Redox Flow Battery Model. Two electrolytic half-cells connected by a membrane that selectively exchanges the ions constitute the VRFB. Pumps connected inside electrolytic tanks provide corresponding ions to the respective electrolytic tanks. The V (5+) and V (4+) ions are stored as electrolytes in the positive half-compartment. The V(3+) and V(2+) ions are present as electrolytes in the negative half-compartment. At the time of discharge, in the positive half-cell, VO2(+) gets converted to VO(2+) ion and in the negative half-cell an electron is liberated from V(2+) to provide V(3+). Reverse reactions take place during charging. Open circuit voltage lies between 1 and 1.6 V. The chemical reactions for charging and discharging are not used in modelling. However, modelling is explained in this section with the help of suitable formulae and Figure 2.

For the VRFB shown, the equation for various parameters can be evaluated as follows:

$$h_{\text{delVs}} = K_{\text{cont}}\left(1 + \frac{V_S^2}{2g}\left(1 - A_{\text{pipe}}\right)^2\right), \tag{1}$$

where Kcont is a constant, V_s is the flow velocity, g is acceleration due to gravity, hdelVs is the enthalpy change due to flow velocity, and Apipe is area of pipes.

$$h_m = K\frac{V_S^2}{2g}, \tag{2}$$

where K is a constant and h_m is the enthalpy change of medium.

$$h_f = 0.316\frac{l}{d}\frac{V_S^2}{2g}, \tag{3}$$

where l and d are dimensions of the container (length and depth), and h_f is the enthalpy of flow of electrolytes.

Now, change in pressure of pipes can be formulated as

$$\text{del.}\,p_{\text{pipes}} = \left[r_o g\left(h_{\text{delVs}} + h_f + h_m\right)\right]. \tag{4}$$

P.pump is then evaluated as

$$P_{\text{.pump}} = \frac{K_i}{Q}\,\text{del.}\,p_{\text{system}}, \tag{5}$$

where Q is the rate of flow of electrolyte, K_i is a constant, and

$$\text{del.}\,p_{\text{system}} = \text{del.}\,p_{\text{stack}} + \text{del.}\,p_{\text{pipes}}, \tag{6}$$

and cell voltage can then be calculated as

$$V_{\text{cell}} = V_{eq} + \frac{2RT}{F}\ln\frac{\text{SOC}}{1 - \text{SOC}}. \tag{7}$$

So, stack voltage comes out to be

$$V_{\text{stack}} = n * V_{\text{cell}}, \tag{8}$$

where N is the number of cells.

Various equations for the given parameters are extracted from [3].

3.2. Fuel Cell Model. Among the various types of fuel cells, PEM fuel cells have gained best response for their operation at low temperature and also because of their fast response time. Fuel cells are one of the most important components for a hybrid power system owing to their inputs which are oxygen and hydrogen, and their output, i.e., water. The modelling of this system is done in SIMULINK using MATLAB functions and the overall model is also available in Simulink Library Browser, as fuel cell stack model. The control circuit in Figure 3 is controlled by the output of blocks B and C which are E_{oc}, i_o, and A. For given values of P_{fuel}, V_{fuel}, Pair, and V_{air}, the above three parameters are determined for a detailed fuel cell stack model by the formulae given in [3].

However, for a simplified fuel cell stack model, the main formula are as follows.

From open circuit voltage E_{oc}, if output voltage is to be determined, then activation losses (owing to kinetics of reactions) and charge transport losses (resistive and diffusion) are to be subtracted to obtain the actual output power, which is

$$V = E_{\text{OC}} - V_{\text{act}} - V_r, \tag{9}$$

with

$$V_{act} = S_t \ln\left(\frac{i_{fc}}{i_o}\right) * \left(\frac{1}{(ST_d/3)} + 1\right),$$
$$V_r = r_{\text{ohm}} * i_{fc}, \tag{10}$$

where S_t is Tafel slope (in V), given by

$$S_t = \frac{RT}{z\alpha F}. \tag{11}$$

α is the charge transfer coefficient. Here, io is the exchanging current (in As), rohm is the cell and diffusion total resistance (in ohms), T_d is settling time required by cell for a current step. Here, it is considered that the cell voltage would have a delay approximately the same as time constant because of sudden change in cell current. So, Tds = 1 second. The stack voltage of a fuel cell when a number of fuel cells are connected is given as the product of individual fuel cell voltage and the number of cells, i.e.,

$$V_{fc} = N_1 * V. \tag{12}$$

Here number of cells is given as N_1.

3.3. Battery Model. Li-ion batteries are considered in this paper owing to their high energy density and highest efficiency (almost 100 percent) compared to other battery

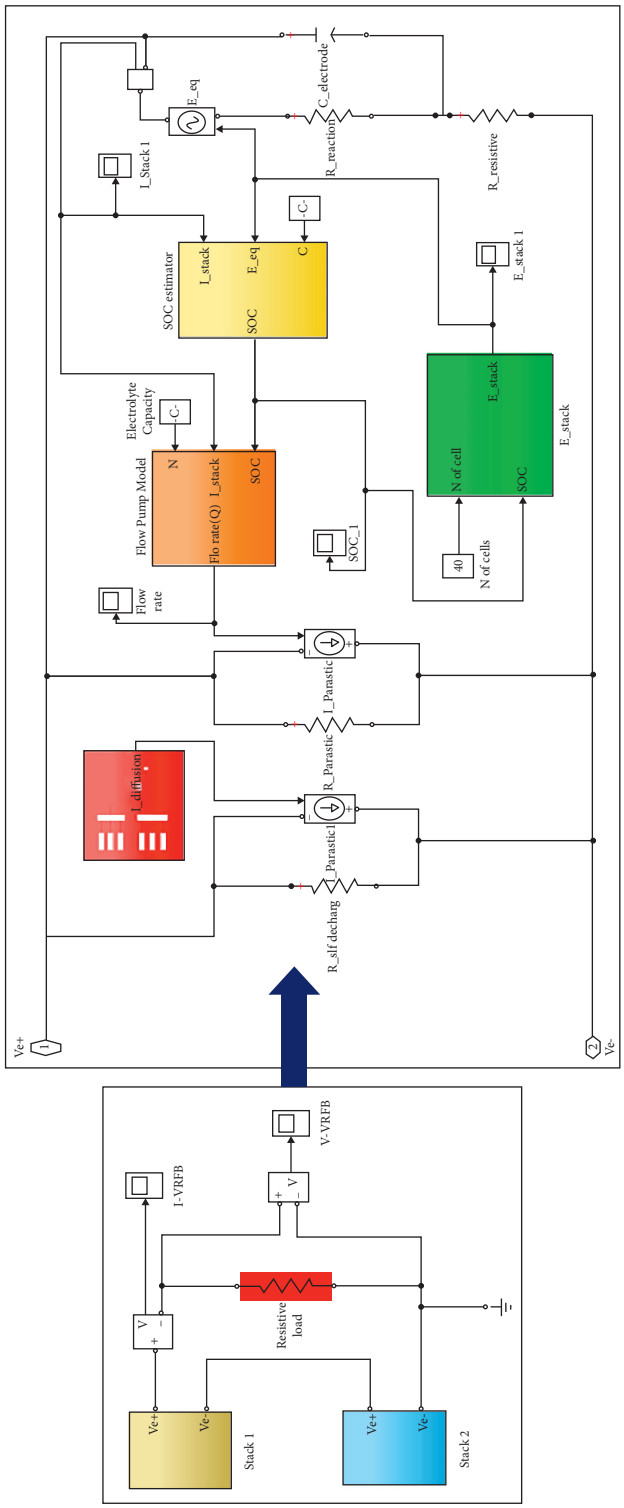

Figure 2: Vanadium Redox Flow Battery simulation model.

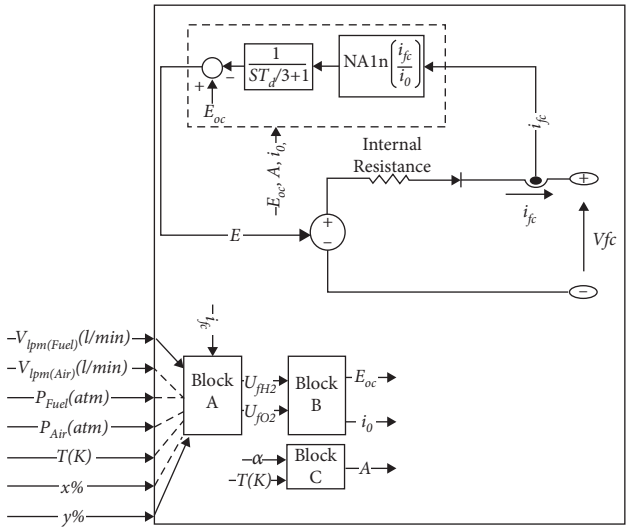

Figure 3: Fuel cell stack model is reproduced from Njoya M et al. 2013.

sources such as Lead Acid (85 percent) and sodium-sulfur (89 percent). The model discussed is available in MATLAB Simulink Library Browser as shown in Figure 4. Shepherd curve fitting method is used where an additional term is added [10]. This enables better representation of the effect of battery SOC on its performance. For stable simulation, battery current is filtered before use, which accounts for polarization resistance. Model parameters can be derived from the data sheet.

The main equations for a Li-ion battery are discussed here.

The V_{batt} is given by

$$V_{batt} = E_0 - K_a \frac{q}{q - It} It - R_b I - A_b \exp(-C * It) - K \frac{q}{q - It} I *, \tag{13}$$

where

(i) E_o = constant battery voltage (in volts)
(ii) K_a = constant of polarization (in V/Ah)
(iii) q = charge capacity (ampere hour)
(iv) $I *$ = battery current filtered (in As)
(v) It = battery charge actual (in Ah)
(vi) A_b = exponential constant (in V)
(vii) C = inverse exponential time constant (in Ah-1)
(viii) R_b = internal R of batt. (in ohms)

The term $K_a(q/q - It) *$ It from (12) is polarized voltage, and the term $K_a(q/q -$ It) is the polarized resistance PolR [11].

The battery voltage increases suddenly when fully charged and this behaviour leads to modification of polarization resistance as follows:

$$\text{Pol}\, R = K_a \left(\frac{q}{It - 0.1q}\right). \tag{14}$$

3.4. Super Capacitor Model. Supercapacitors structures are similar to conventional electrolytic capacitors. Additionally, it has a property to store or release more energy in small instances of time due to their high capacitance [12]. Owing to this property, it is used here to operate in transient state for voltage regulation. SC compensates for high frequency component of fast changing power peaks and also compensates for the uncompensated battery power (due to slow dynamics of battery) as shown in Figure 5. The supercapacitors model presented here is made in MATLAB using MATLAB function block and is based on the Stern model, which combines the Helmholtz and Gouy-chapman models [4]. The capacitance of an SC cell is expressed as

$$C = \frac{1}{(1/C_H) + (1/C_{GC})}, \tag{15}$$

with

$$C_H = \frac{N_C e e_0 A_i}{d},$$
$$C_{GC} = \frac{F q_C}{2 N_C RT} \sinh\left(\frac{q_c}{\left(N^C\right)^2 A_i (8RTee_0 c)^{0.5}}\right), \tag{16}$$

where C_H = Helmholtz capacitance (in F), CGC = Gouy-Chapman capacitance (in F), N_c = Number of electrode layers, e = Permittivity value (in F/m) of the electrolytic material used, e_o = Permittivity value (in farads per meter) of free space, A_i = Interfacial area between the electrode and electrolytes (in meter-square), d = radius of molecules (in m), q_c = electric charge of each cell (in Coulomb), and c = Molar concentrations (in moles per meter cube).

For a supercapacitor module, with N_s cells in series and N_p cells in parallel, the total capacitance is given as

$$C_T = \frac{N_P}{N_S} C. \tag{17}$$

When V_{sc} is measured by taking into account the losses (due to resistance), it comes out as

$$V_{\text{SC}} = \frac{Q_T}{C_T} - R_{\text{SC}} i_{\text{sc}}, \tag{18}$$

with

$$Q_T = N_P Q_C = \int i_{\text{sc}} \mathrm{d}t, \tag{19}$$

where Q_T = Total electric charge (in coulombs), R_{SC} = Total SC resistance (in ohms), and i_{SC} = SC module current (in amperes).

3.5. DC-DC Converter Model. The VRFB, FC power module, and battery system are connected to load through DC/DC converters and DC/AC converter as shown in Figures 6 and 7. DC/DC converters are used for voltage conversion in the case of charging and discharging. In the case of fuel cell, we use boost converter, and Li-ion battery has both buck (charge converter) and boost (discharge converter)

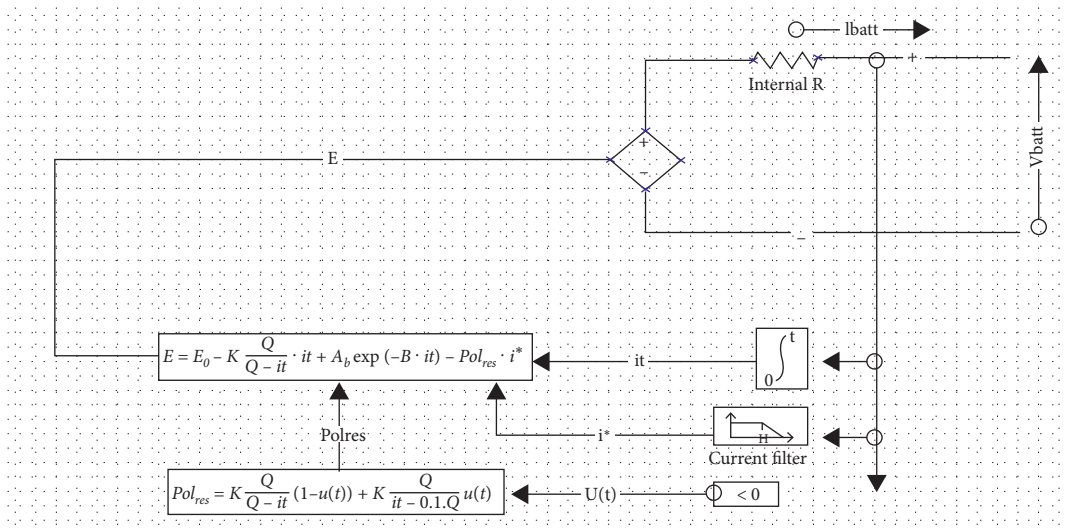

Figure 4: Li-ion battery model.

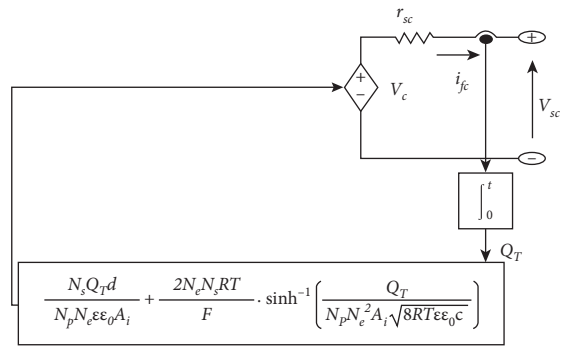

Figure 5: Supercapacitor model.

converter [13]. The VRFB system has a DC/DC bidirectional converter.

Here DC/DC converters are operating in switching mode, which are mainly used for design purpose. In this paper by the help of PI controller and filters we generate duty signals (pulse width modulated signals) by comparing DC bus voltages and reference voltages; these signals are further used to operate the switch of converters [14].

3.6. DC/AC Converter Model. The DC/AC converter model is represented in the same way as in the DC/DC converter models, i.e., through average value models as shown in Figures 8 and 9. As most of the loads are AC in nature, here, the obtained output of the system is converted into AC to feed the load demand [15]. A reference voltage signal is used to generate controlled voltage source signal and the input current is generated from output power and DC bus voltage.

3.7. Load Profile. For experimental purpose, we have 3-phase AC electronically programmable load. Here load current is obtained by three-phase apparent power (in KVA), the nominal line voltage, and its power factor [16].

3.8. EM Scheme. The EMS is used to ensure the following:

(i) minimization of voltage spikes
(ii) low consumption of hydrogen fuel
(iii) enhancing efficiency of system
(iv) minimum variation in battery/VRFB/super-capacitor SOC
(v) higher durability
(vi) in this paper we are using adaptive P and I control minal line voltage, and its power strategy
(vii) adaptive P and I control strategy

Adaptive P and I controller are used to control the SOC level of batteries. It modifies the error between reference SOC and obtained SOC with the help of PI controller and saturator blocks. If SOC level is above reference and at the same point VRFB power is below the required value, then PI controller allows battery to

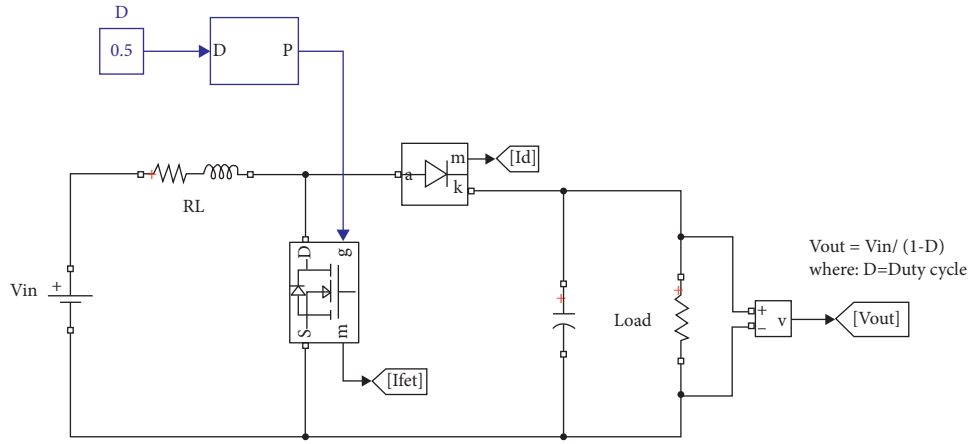

Figure 6: Boost converter model.

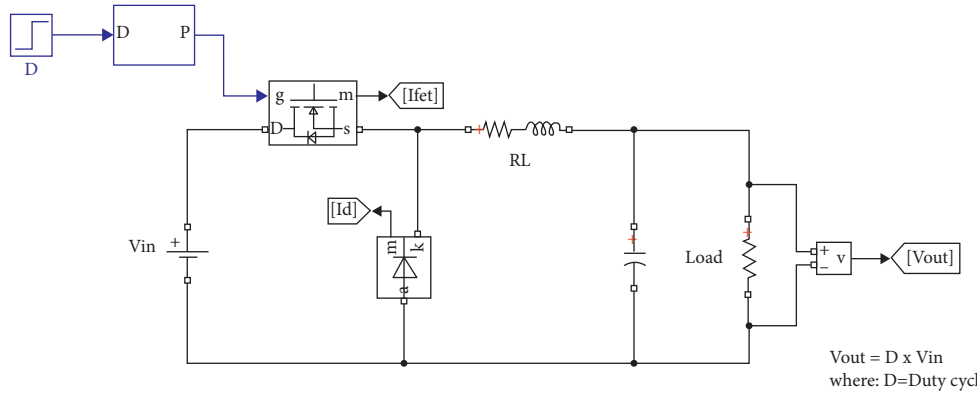

Figure 7: Buck converter model.

provide its full power to DC buses [5]. If SOC is below reference then controller generates duty for its charging; in this case VRFB provides power to load. Adaptive P + I controller energy management can be implemented easily as compared to others.

4. Simulation and Experimental Results

In order to understand the performance of the hybrid power system and control, a simple islanded DC microgrid network as shown in Figure 1 is simulated using MATLAB/SIMULINK software. In this paper adaptive P and I controller are used to control the SOC level of batteries. There are a lot of investigations proposing microgrids for country charge applications in creating nations. For instance, creators talked about the past and current practices to further develop energy access, as well as advancing country charge utilizing microgrids in China, India [17]. The system has been tested with various conditions and its results have been plotted in Figures 10–12 showing the gate pulse waveforms for buck and boost converter. The DC microgrid system with buck/boost converter along with conventional and adaptive PI controller hardware results for SOC of the battery is shown in Figures 13(a)–13(e). The converter output voltage waveform is shown in Figure 14.

The DC-DC buck converter is displayed in MATLAB/SIMULINK with the reproduction result of the converter. The simulation output shows that the planned DC-DC buck convertor controls and lessens the input voltage. The simulation parameters are as shown in Table 1.

Most batteries are intended to work in the condition of charge scope of 20–90%. Subsequently, the methodology in the regulator will check assuming that the batteries are in the scope of 20–90%. Other than that, the battery regulator is relying upon the power age and burden interest. In the event that the power produced is higher than the required load power and the battery is at a low SOC underneath 90% the battery will be charged [6]. Nonetheless, on the off chance that the heap power is higher than the created power load shedding ought to be thought about to safeguard the wellbeing of the battery [7]. Likewise, in the event that the produced power is more noteworthy than the power load and SOC is in the scope of 20% to 90% the battery will be charged except if the battery ought to be released [18].

AC microgrids require more parts, and the outcomes acquired in this study are unique. As a result of the expected inverters, there will be extra power misfortunes that lead to an alternate PV and battery estimating to adjust the stock and the interest [8]. As overreleasing the battery routinely will cause its time span of usability to

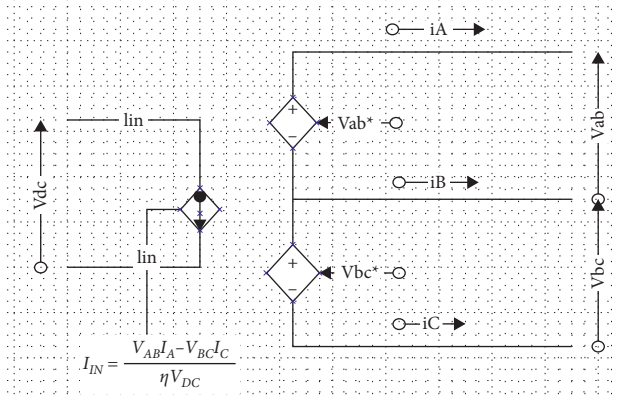

Figure 8: DC/AC converter model.

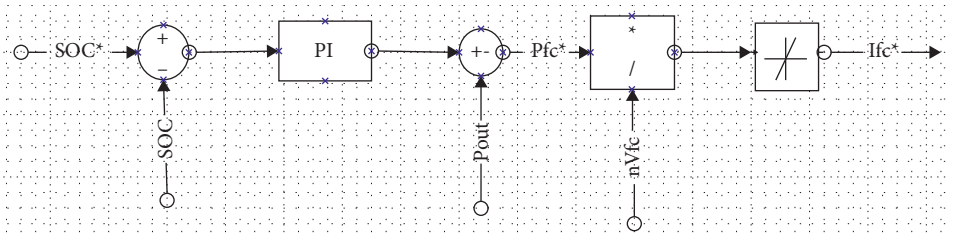

Figure 9: Adaptive $P+I$ control strategy.

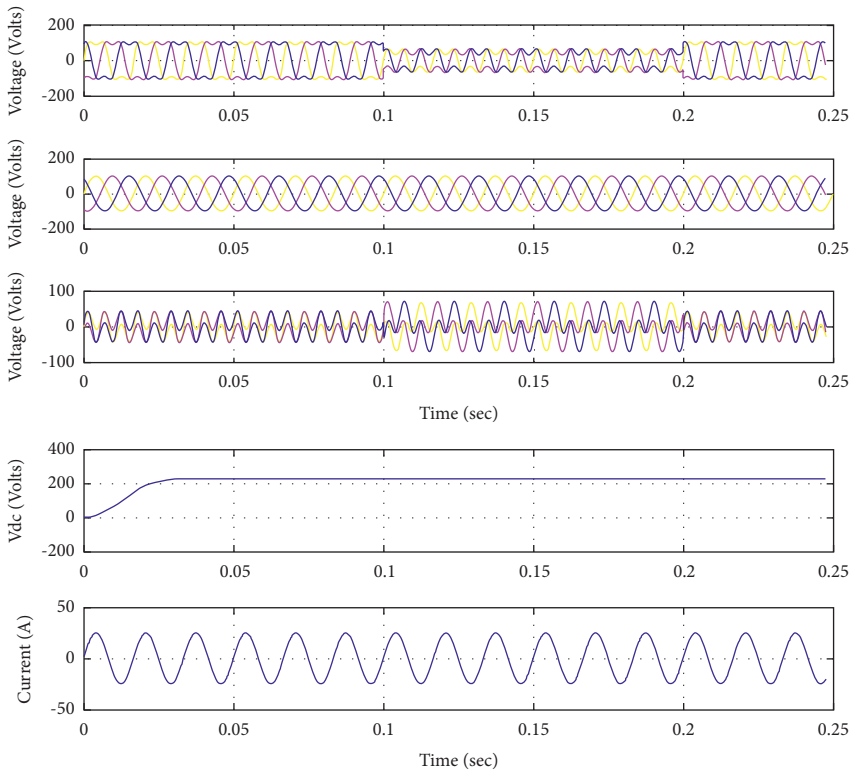

Figure 10: DC voltage and its compensation current in simulation.

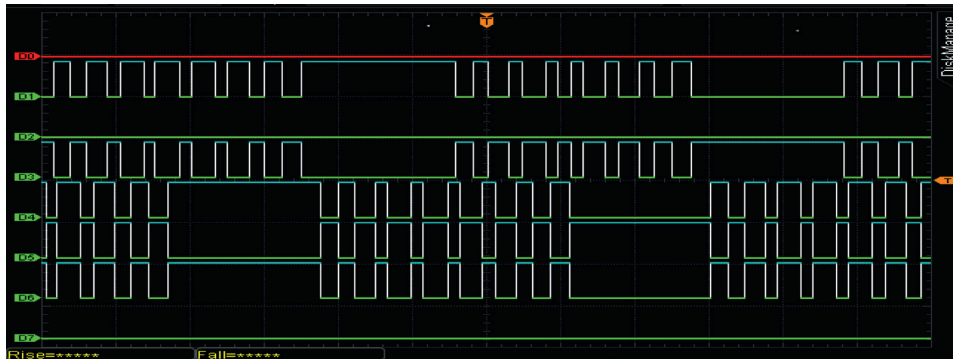

Figure 11: Buck converter gate pulse.

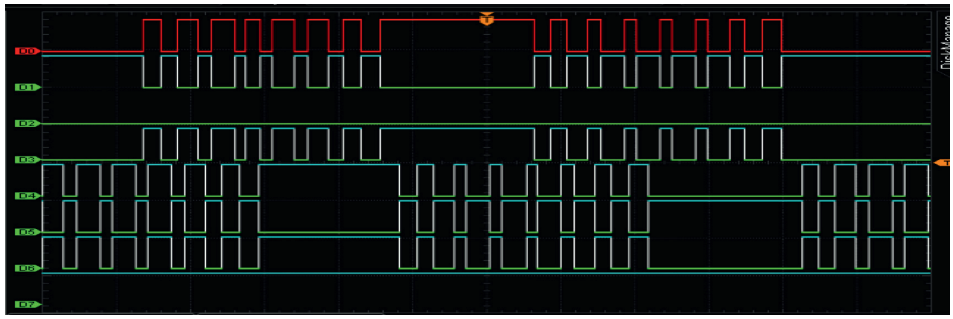

Figure 12: Boost converter gate pulse.

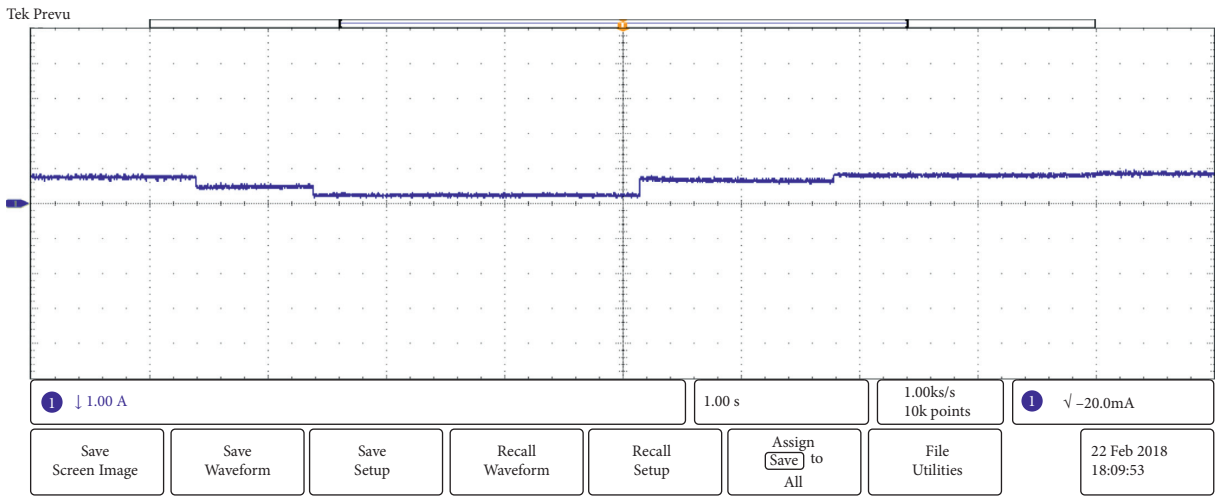

(a)

Figure 13: Continued.

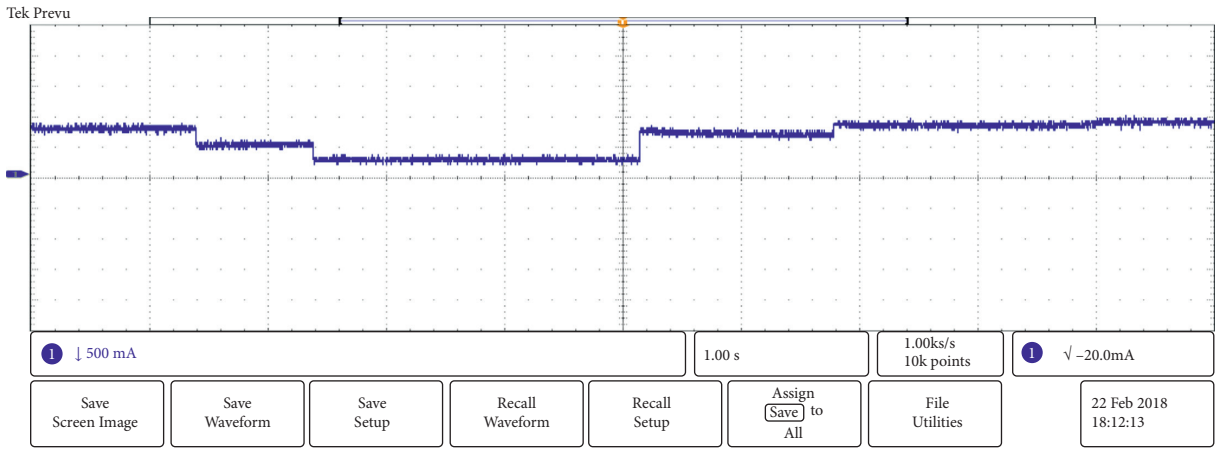

(b)

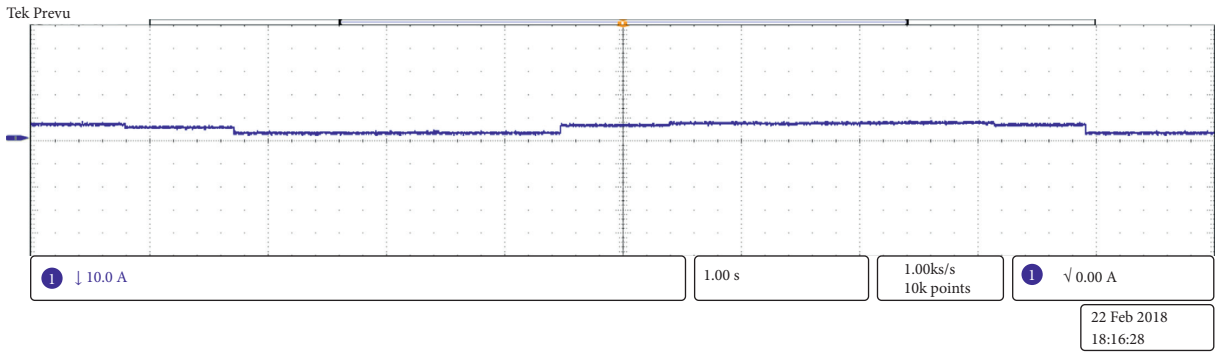

(c)

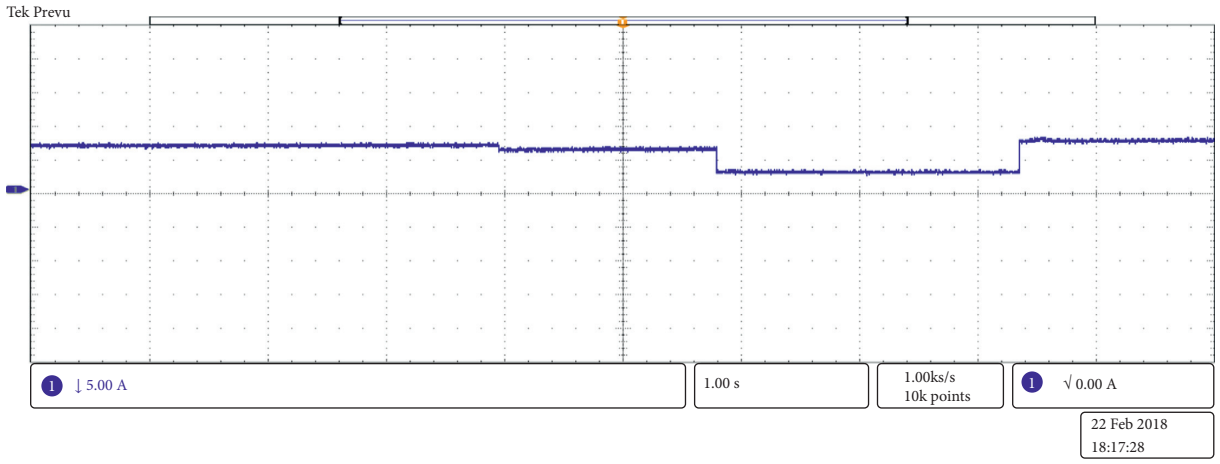

(d)

Figure 13: Continued.

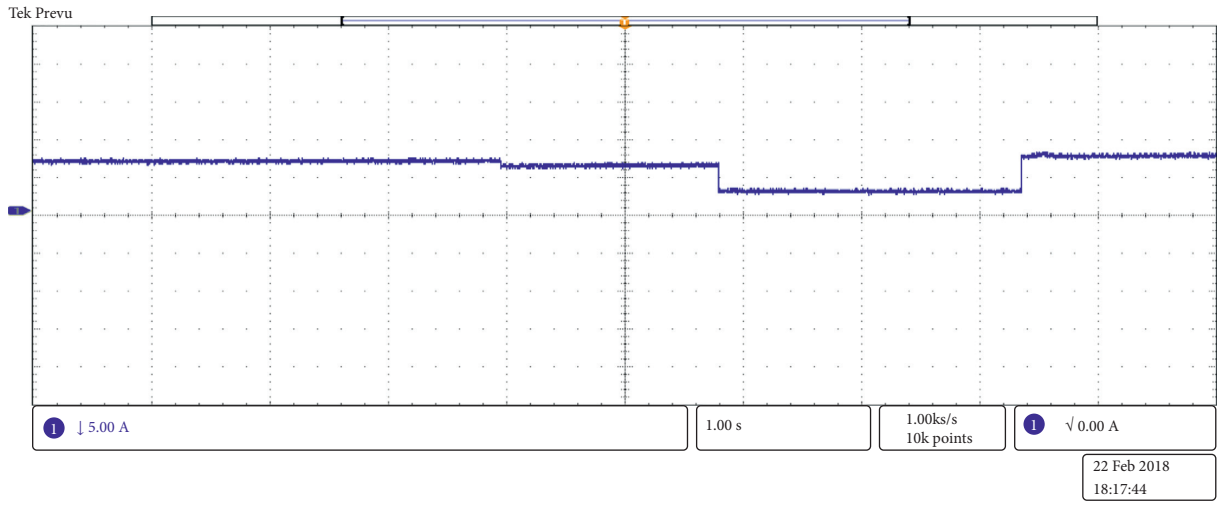

(e)

Figure 13: Islanded DC microgrid network with PI controller and adaptive PI controller investigated with SOC level of batteries. (a) Charge control with conventional control scheme. (b) Charge control with conventional control scheme and buck converter. (c) Charge control with conventional control scheme and boost converter. (d) Charge control with adaptive PI controller. (e) Charge control with adaptive PI controller and buck converter.

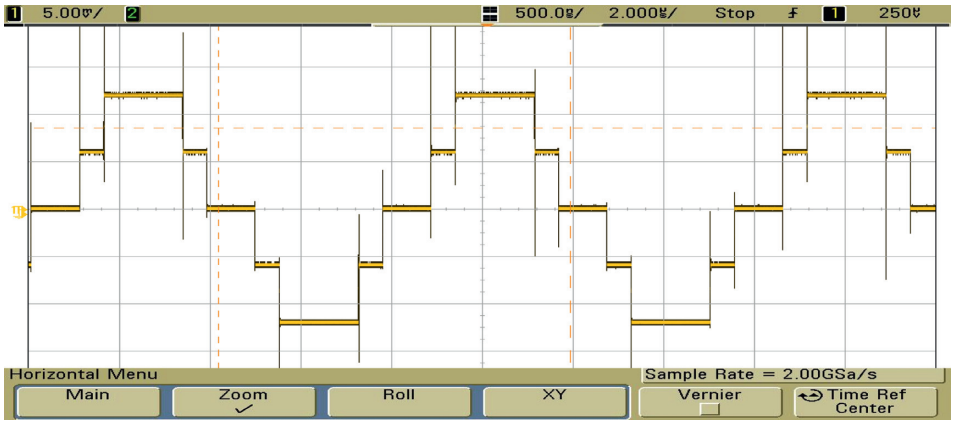

Figure 14: Output voltage waveform obtained from converter.

Table 1: Simulation parameters of DC grid are reproduced from Beykverdi et al. 2016.

Parameter	Symbol	Value
Dc bus voltage	V_{dc}	230 V
Low threshold DC voltage	V_L	212 V
High threshold DC voltage	V_H	235 V
Battery capacity	C_{bat}	50 Ah
Initial SOC	SOC	65%
Maximum SOC	SOC_{max}	90%
Minimum SOC	SOC_{min}	20%

abbreviate, the power device may be actuated when certain conditions are met. Charge regulators are vital in BIPV frameworks to keep batteries from being harmed by cheating and overreleasing by controlling the current stream from and to the batteries [9]. They can likewise safeguard the machines that are associated with the batteries in BIPV frameworks. Most batteries can scarcely recuperate in the wake of cheating and overreleasing, so the work of regulators in BIPV frameworks can delay the assistance life of the batteries.

5. Conclusions

An energy management scheme for an islanded DC microgrid with VRFB hybrid system has been presented. The hybrid system is modelled and validation is provided through experiments. The voltage spikes due to sudden change in load have been regulated by using supercapacitor and Li-ion battery integrated with VRFB. To reduce fuel consumption, adaptive P and I control strategy is used. Vanadium redox stream battery (VRFB) frameworks are the most evolved among stream batteries in light of their dynamic species staying in arrangement consistently during charge/release cycling, their high reversibility, and their somewhat enormous power yield. Be that as it may, the capital expense of these frameworks stays very high for profound market entrance. To meet the proposed cost targets, ongoing examinations have featured the utilization of natural dynamic materials in strong state natural batteries, in which energy is put away inside the cell, principally as an extreme polymer.

Data Availability

The required data can be obtained from the corresponding author upon request.

Conflicts of Interest

The authors declare that they have no conflicts of interest.

References

[1] S. N. Motapan, L.-A. Dessaint, and K. Al-Haddad, "A comparative study of energy management schemes for a fuel-cell hybrid emergency power system of a more-electric aircraft," *IEEE Transactions on Industrial Electronics*, vol. 61, no. 3, 2014.

[2] P. Thounthong and S. Rael, "The benefits of hybridisation," *IEEE Ind. Electron Mag.*vol. 3, no. 3, pp. 25–37, 2009.

[3] W. Wei Jiang and B. Fahimi, "Active current sharing and source management in fuel cell-battery hybrid power system," *IEEE Transactions on Industrial Electronics*, vol. 57, no. 2, pp. 752–761, 2010.

[4] K. B. Oldham, "A Gouy-Chapman-Stern model of the double layer at a (metal)/(ionic liquid) interface," *Journal of Electroanalytical Chemistry*, vol. 613, no. 2, pp. 131–138, 2008.

[5] G. Peter and S. Bin Iderus, "Design of enhanced energy meter using GSM prepaid system and protective relays," *Materials Today Proceedings*, vol. 39, pp. 582–589, 2021.

[6] N.-G. Lim, H.-W. Song, H.-H. Jung, and S. Lee, "A study on capacity estimation of VRFB system using cumulated charge," *The Transactions of the Korean Institute of Electrical Engineers*, vol. 70, no. 9, pp. 1304–1311, 2021.

[7] Z. Huang, A. Mu, L. Wu, and H. Wang, "Vanadium redox flow batteries: flow field design and flow rate optimization," *Journal of Energy Storage*, vol. 45, Article ID 103526, 2022.

[8] P. Geno Peter and M. Rajaram, "An enhanced Z-source inverter topology-based permanent magnet brushless DC motor drive speed control," *International Journal of Electronics*, vol. 102, no. 8, pp. 1289–1305, 2015.

[9] M. Boselli, F. Cavrini, V. Colombo et al., "High-Speed and schlieren imaging of a low power inductively coupled plasma source for potential biomedical applications," *IEEE Transactions on Plasma Science*, vol. 42, no. 10, pp. 2748-2749, 2014.

[10] C.-T. Liu, K.-Y. Cheng, Z.-H. Lin, C.-J. Wu, J.-Y. Wu, and J.-S. Wu, "Effect of ground and floating electrode on a helium-based plasma jet and its applications in sterilization and ceramic surface treatment," *IEEE Transactions on Plasma Science*, vol. 44, no. 12, pp. 3196–3200, 2016.

[11] S. Wu, Y. Cao, and X. Lu, "The state of the art of applications of atmospheric-pressure nonequilibrium plasma jets in dentistry," *IEEE Transactions on Plasma Science*, vol. 44, no. 2, pp. 134–151, 2016.

[12] G. Peter and A. Sherine, "Induced over voltage test on transformers using enhanced Z-source inverter based circuit," *Journal of Electrical Engineering*, vol. 68, no. 5, pp. 378–383, 2017.

[13] J. Florian, N. Merbahi, G. Wattieaux, J.-M. Plewa, and M. Yousfi, "Comparative studies of double dielectric barrier discharge and microwave argon plasma jets at atmospheric pressure for biomedical applications," *IEEE Transactions on Plasma Science*, vol. 43, no. 9, pp. 3332–3338, 2015.

[14] Y.-J. Kim, S. Jin, G.-H. Han et al., "Plasma apparatuses for biomedical applications," *IEEE Transactions on Plasma Science*, vol. 43, no. 4, pp. 944–950, 2015.

[15] K. H. Becker, B. B. Godfrey, E. E. Kunhardt et al., "Robert barker memorial session: leadership in plasma science and applications," *IEEE Transactions on Plasma Science*, vol. 43, no. 4, pp. 914–936, April 2015.

[16] G. Peter, K. Praghash, A. Sherine, and V. Ganji, "A combined PWM and AEM-based AC voltage controller for resistive loads," *Mathematical Problems in Engineering*, vol. 2022, 11 pages, Article ID 9246050, 2022.

[17] G. Peter, A. Sherine, and S. B. Iderus, "Enhanced Z-source inverter-based voltage frequency generator to conduct induced over voltage test on power transformers," *International Journal of Power Electronics*, vol. 12, no. 4, p. 493, 2020.

[18] X. Lu and A. Fridman, "Guest editorial the second special issue on atmospheric pressure plasma jets and their applications," *IEEE Transactions on Plasma Science*, vol. 43, no. 3, pp. 701-702, 2015.